



Interaction of Thioflavin T with amyloid fibrils of apolipoprotein A-I N-terminal fragment: Resonance energy transfer study



Mykhailo Girych^{a,*}, Galyna Gorbenko^a, Valeriya Trusova^a, Emi Adachi^b, Chiharu Mizuguchi^b, Kohjiro Nagao^b, Hiroyuki Kawashima^c, Kenichi Akaji^c, Sissel Lund-Katz^d, Michael C. Phillips^d, Hiroyuki Saito^b

^a Department of Nuclear and Medical Physics, V.N. Karazin Kharkiv National University, 4 Svobody Sq., Kharkov 61077, Ukraine

^b Institute of Health Biosciences, Graduate School of Pharmaceutical Sciences, The University of Tokushima, 1-78-1 Shomachi, Tokushima 770-8505, Japan

^c Department of Medicinal Chemistry, Kyoto Pharmaceutical University, Yamashina-ku, Kyoto 607-8412, Japan

^d Lipid Research Group, Gastroenterology, Hepatology and Nutrition Division, The Children's Hospital of Philadelphia, Perelman School of Medicine at the University of Pennsylvania, Philadelphia, PA 19104-4318, United States

ARTICLE INFO

Article history:

Received 6 March 2013

Received in revised form 8 October 2013

Accepted 25 October 2013

Available online 15 November 2013

Keywords:

Amyloid fibrils

ApoA-I N-terminal fragment

Thioflavin T

Förster resonance energy transfer

ABSTRACT

Apolipoprotein A-I is amenable to a number of specific mutations associated with hereditary systemic amyloidosis. Amyloidogenic properties of apoA-I are determined mainly by its N-terminal fragment. In the present study Förster resonance energy transfer between tryptophan as a donor and Thioflavin T as an acceptor was employed to obtain structural information on the amyloid fibrils formed by apoA-I variant 1-83/G26R/W@8. Analysis of the dye-fibril binding data provided evidence for the presence of two types of ThT binding sites with similar stoichiometries (bound dye to monomeric protein molar ratio ~10), but different association constants (~6 and 0.1 μM^{-1}) and ThT quantum yields in fibril-associated state (0.08 and 0.05, respectively). A β -strand-loop- β -strand structural model of 1-83/G26R/W@8 apoA-I fibrils has been proposed, with potential ThT binding sites located in the solvent-exposed grooves of the N-terminal β -sheet layer. Reasoning from the expanded FRET analysis allowing for heterogeneity of ThT binding centers and fibril polymorphism, the most probable locations of high- and low-affinity ThT binding sites were attributed to the grooves T16_Y18 and D20_L22, respectively.

© 2013 Elsevier Inc. All rights reserved.

1. Introduction

An intrinsic propensity of polypeptide chains for self-assembly into highly ordered aggregates (amyloid fibrils) currently attracts ever growing interest in a variety of research areas, from biomedicine (Zerovnik, 2002; Stefani, 2004) to nanotechnologies (Knowles and Buehler, 2011; Mankar et al., 2011). At the molecular level, amyloid fibrils possess a core cross- β -sheet structure, with β -strands running perpendicularly to the long axis of the fibril and β -sheets propagating in its direction (Makin and Serpell, 2005). This architecture gives rise to a characteristic X-ray diffraction pattern with 4.8 and 10 Å reflections, corresponding to inter-strand spacing within β -sheet and separation between β -sheet layers, respectively (Nelson and Eisenberg, 2006). The conversion of specific proteins into amyloid fibrils proved to be associated with a number of pathological conditions, including neurological diseases, type II diabetes, spongiform encephalopathies, systemic amyloidosis, etc. (Stefani, 2004; Idicula-Thomas and Balaji, 2007).

* Corresponding author. Address: 19/2 Tankopiya Str., Kharkov 61091, Ukraine.
E-mail address: girichms@gmail.com (M. Girych).

One of the most common ways of identification and quantification of fibrillar aggregates is based on monitoring the fluorescence changes of the benzothiazole dye Thioflavin T (ThT) (Naiki et al., 1989). The interaction of this dye with amyloid fibrils is followed by significant long-wavelength shifts of its excitation and emission maxima, coupled with a dramatic (up to several orders of magnitude) increase in fluorescence intensity (LeVine, 1993; Groenning, 2010). An unprecedented enhancement of ThT fluorescence is supposed to originate from restricted torsional oscillations of the benzothiazole and aminobenzoyl rings of the dye molecule upon its incorporation in the solvent-exposed grooves spanning across consecutive β -strands parallel to the fibril axis (Sulatskaya et al., 2010; Stsiapura et al., 2007; Hawe et al., 2008). This binding mode hinders the formation of a weakly-radiative twisted internal charge-transfer state and causes ThT to adopt a nearly planar conformation (Stsiapura et al., 2007). Recent atomic level studies of ThT-fibril interactions revealed ThT amino acid sequence specificity, viz. its preferential association with the grooves lined with aromatic residues (Biancalana and Koide, 2010). A variety of remarkable properties of ThT render this dye highly suitable not only for detecting the presence of amyloid fibrils, but also for

structural characterization of this type of protein aggregate. To gain further insights into molecular determinants of amyloid specificity, it is reasonable to systematically examine ThT binding to amyloid fibrils assembled from proteins differing in their structural and physicochemical characteristics.

Apolipoprotein A-I (apoA-I) is the major protein component of high-density lipoproteins promoting efflux of phospholipid and cholesterol from plasma membrane (Phillips, 2013). Specific variants of human apoA-I, particularly those having G26R substitution mutation, are capable of forming amyloid fibrils associated with renal or liver failure (Joy et al., 2003). The N-terminal fragment has been identified as the predominant form of apoA-I in amyloid fibril deposits (Nichols et al., 1990; Lagerstedt et al., 2007). In fact, it was recently demonstrated that the N-terminal 1–83 fragment of apoA-I has a strong propensity to form amyloid fibrils at physiological neutral pH (Adachi et al., 2013). However, the structural characterization of amyloid fibrils of apoA-I is still lacking.

In the present study we explored ThT interactions with fibrillar N-terminal fragment (amino acids 1–83) of apoA-I, using the Förster resonance energy transfer (FRET) technique. This fragment contains three tryptophan residues, Trp8, Trp50 and Trp72. One of these intrinsic fluorophores, Trp8, was recruited as energy donor for ThT in the FRET experiments, while two other Trp residues were substituted by Phe, yielding the apoA-I single Trp variant at Trp8. Our goal was threefold: (i) to obtain quantitative characteristics of ThT complexation with fibrillar protein (association constant, binding stoichiometry, quantum yield of the bound dye); (ii) to estimate Trp8–ThT separation and (iii) to define possible locations of the dye within the fibril structure.

2. Materials and methods

2.1. ApoA-I proteins

The N-terminal 1–83 fragment of human apoA-I G26R, its single tryptophan variant 1–83/G26R/W@8 and 1–83/G26R/D48A/W@8 were expressed and purified as described (Adachi et al., 2013). Since two extra amino acids, Gly and Ser, are attached at the amino terminus of the target apoA-I, the two residues preceding the normal apoA-I sequence are numbered –1 and –2. The apoA-I preparations were at least 95% pure as assessed by SDS–PAGE.

2.2. Preparation of apoA-I fibrils

In all experiments, 1–83/G26R/W@8 and 1–83/G26R/D48A/W@8 apoA-I variants were freshly dialyzed from 6 M guanidine hydrochloride solution into 10 mM Tris buffer (150 mM NaCl, 0.01% NaN₃, pH 7.4) before use. The reaction of apoA-I fibrillization was carried out at 37 °C in the above buffer with constant agitation on an orbital shaker. The amyloid nature of fibrillar aggregates was confirmed with the ThT assay (Groenning, 2010).

2.3. Fluorescence measurements

Fluorescence measurements were performed with a LS-55 spectrofluorimeter equipped with a magnetically stirred cuvette holder (Perkin-Elmer Ltd., Beaconsfield, UK) using 10 mm path-length quartz cuvettes. The apoA-I Trp fluorescence was selectively excited at 296 nm, where the extinction coefficient of Trp ($\epsilon_{296} \sim 1.5 \times 10^3 \text{ M}^{-1} \text{ cm}^{-1}$) is significantly greater than that of Tyr ($\epsilon_{296} \sim 30 \text{ M}^{-1} \text{ cm}^{-1}$) (Lakowicz, 2006). Excitation and emission band passes were set at 10 nm. ThT fluorescence was recorded from 450 to 600 nm at an excitation wavelength of 420 nm.

The efficiency of resonance energy transfer between Trp as a donor and ThT as an acceptor was determined by comparing the

sensitized emission of the acceptor with the residual donor emission (Selvin, 1996):

$$Q_r = 1 - E = \frac{I_{DA}q_A}{I_{DA}q_A + I_{AD}q_D} \quad (1)$$

where I_{AD} is the integrated area of the sensitized emission of the acceptor, I_{DA} is the integrated area under the donor emission curve in the presence of the acceptor, q_D is the quantum yield of the donor, and q_A is the quantum yield of the acceptor. The protein fluorescence intensity measured in the presence of ThT was corrected for inner filter effect using the following coefficients (Bulychev et al., 1988):

$$k = \frac{(1 - 10^{-A_o^{ex}})(A_o^{ex} + A_a^{ex})}{(1 - 10^{-(A_o^{ex} + A_a^{ex})})A_o^{ex}} \frac{(1 - 10^{-A_o^{em}})(A_o^{em} + A_a^{em})}{(1 - 10^{-(A_o^{em} + A_a^{em})})A_o^{em}} \quad (2)$$

where A_o^{ex} , A_o^{em} are the donor optical densities at the excitation and emission wavelengths in the absence of acceptor, A_a^{ex} , A_a^{em} are the acceptor optical densities at the excitation and emission wavelengths, respectively.

The critical distance of energy transfer was calculated as (Lakowicz, 2006):

$$R_0 = 979(\kappa^2 n_r^{-4} Q_D J)^{1/6}, \quad J = \int_0^\infty F_D(\lambda) \epsilon_A(\lambda) \lambda^4 d\lambda / \int_0^\infty F_D(\lambda) d\lambda \quad (3)$$

where J is the overlap integral derived from numerical integration, $F_D(\lambda)$ is the donor fluorescence intensity, $\epsilon_A(\lambda)$ is the acceptor molar absorbance at the wavelength λ , n_r is the refractive index of the medium ($n_r = 1.4$), Q_D is the donor quantum yield, κ^2 is an orientation factor. The quantum yields of the apoA-I Trp and ThT were estimated using tryptophan solution in water ($Q = 0.14$) and ethanol solution of 4-dimethylaminostyryl-1-hexylpyridinium ($Q = 0.05$) as standards, respectively. Assuming random reorientation of the donor emission and acceptor absorption transition moments during the emission lifetime ($\kappa^2 = 0.67$), R_0 value was estimated to be 2.9 nm for Trp–ThT donor–acceptor pair (with $Q_D = 0.13$ for apoA-I Trp).

2.4. Atomic force microscopy (AFM)

Measurement by AFM was carried out with a NanoScope[®] IIIa scanning probe work station equipped with a MultiMode head using an E-series piezoceramic scanner (Digital Instruments, Santa Barbara, CA, USA). AFM probes were single-crystal silicon micro cantilevers with 300 kHz resonant frequencies and 26 N/m spring constant model OMCL-AC160TS-R3 (Olympus, Tokyo, Japan). 10 μL of each sample solution was spotted on freshly cleaved mica (The Nilaco Co., Tokyo, Japan). After washing the mica with distilled water (20 μL), samples were imaged under ambient conditions at room temperature at scan rates of 0.5 Hz by tapping mode.

2.5. Circular dichroism (CD) measurements

Far-UV CD spectra were recorded from 185 to 260 at 25 °C using a Jasco J-600 spectropolarimeter. The apoA-I solutions of 50 $\mu\text{g/ml}$ in 10 mM Tris buffer (pH 7.4) were subjected to CD measurements in a 2-mm quartz cuvette, and the results were corrected by subtracting the buffer base line.

2.6. Generation of structural model

A structural model of fibrillar 1–83 apoA-I N-terminal fragment was generated by energy minimization runs in Rosetta (Delano, 2005). The initial conformation of apoA-I variant was constructed in MOLMOL (Koradi et al., 1996) with backbone torsion angles ϕ

(ϕ) = -140° and $\psi = 140^\circ$ for residues 14–31 and 41–58, and those chosen manually for residues 1–13, 32–40 and 59–83. Four copies of the apoA-I fragment were combined allowing for 0.47 nm displacement along the direction of intermolecular hydrogen bonds for the β -strand segments. The structures resulting from the subsequent restrained energy minimization were depicted using the VMD molecular visualization program (Humphrey et al., 1996).

3. Results and discussion

3.1. Analysis of ThT binding data

As shown in Fig. 1, fibrillization of apoA-I variant was followed by a drastic increase in ThT fluorescence, of more than three orders of magnitude. To characterize the process of ThT–fibril binding quantitatively, we employed the method of double fluorimetric titration based on measuring the increment of ThT fluorescence at either varying protein or dye concentration. Allowing for structural complexity of the examined system, while choosing the adsorption model for data analysis we proceed from the notion that the most adequate model should be the simplest and most statistically significant one. Therefore, we started from the simplest Langmuir adsorption model considering one class of binding centers (one-site model). To quantify the amount fibril-associated ThT, it was assumed that the fluorescence intensity increase (ΔI) observed at the formation of ThT-protein complex (Fig. 2) is proportional to the concentration of bound dye (B_z):

$$\Delta I = I - I_0 = aB_z \quad (4)$$

where I_0 is the dye fluorescence intensity in a buffer, a is a coefficient proportional to the difference of ThT quantum yields in a buffer and protein-associated state. In terms of the Langmuir adsorption model the concentration of bound dye can be represented as a function of the total concentrations of the dye (Z) and protein (P), association constant (K_a) and binding stoichiometry (n , in mol of ThT per mole of protein) using the following relationship:

$$K_a = \frac{B_z}{(Z - B_z)(nP - B_z)} = \frac{B_z}{F_z(nP - B_z)} \quad (5)$$

where F_z is the concentration of free dye. Scatchard transformation of this expression into the form $B_z/F_z = f(B_z)$ is commonly used to assess the validity of one-site adsorption model. To obtain Scatchard transform, we employed the double reciprocal plot $1/\Delta I$ vs. $1/P$ (Fig. 3A). In the case when $nP \gg B_z$, from Eqs. (4) and (5) it follows that:

$$\frac{1}{\Delta I} = \frac{1}{anPK_a Z} + \frac{1}{aZ} \quad (6)$$

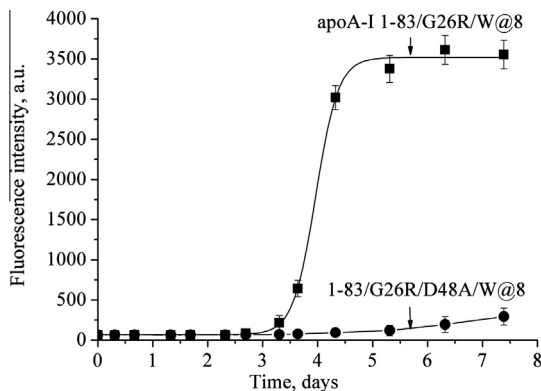


Fig. 1. Fibrillization kinetics of apoA-I 1-83/G26R/W@8 and 1-83/G26R/D48A/W@8 apoA-I variants monitored by measuring ThT fluorescence intensity at 484 nm. Protein concentration was 0.9 μ M, ThT concentration was 6.9 μ M.

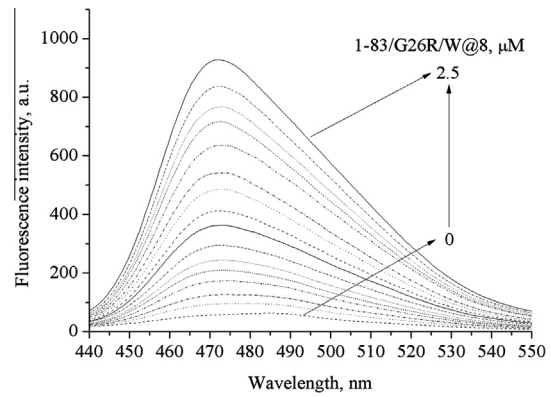


Fig. 2. Emission spectra of ThT recorded at increasing concentrations of apoA-I variant 1-83/G26R/W@8. ThT concentration was 0.17 μ M.

The y-intercept of the $1/\Delta I$ vs. $1/P$ equals $1/aZ$ thus yielding an approximate value of a required for calculation of B_z from Eq. (4). As seen in Fig. 3B, Scatchard transform of the $\Delta I(Z)$ binding curve has a concave-up appearance suggestive of the existence of more than one population of ThT binding sites. Therefore, ThT–fibril binding data were analyzed in terms of two-site binding model, described by the following relationships:

$$\Delta I = a_1 B_{z1} + a_2 B_{z2}; \quad B_1 = \frac{n_1 PK_{a1}(Z - B_{z1} - B_{z2})}{1 + K_{a1}(Z - B_{z1} - B_{z2})};$$

$$B_2 = \frac{n_2 PK_{a2}(Z - B_{z1} - B_{z2})}{1 + K_{a2}(Z - B_{z1} - B_{z2})} \quad (7)$$

where subscripts 1,2 correspond to the binding centers of the first and second class, respectively.

To determine the binding parameters we employed the global fitting approach involving simultaneous analysis of three datasets ($N = 57$ data points) obtained upon varying either ThT (Fig. 3C) or protein concentration (Fig. 3D). The ΔI values calculated from the Eqs. (4) and (7) (ΔI_i^{theor}) were fitted to the experimental ΔI values (ΔI_i^{exp}) through minimization of the function:

$$f = \frac{1}{N} \sum_{i=1}^N \left(\frac{\Delta I_i^{exp}}{\Delta I_i^{theor}} - 1 \right)^2 \quad (8)$$

The general problem encountered in multiparametric data fitting is associated with cross-correlation between the optimizing parameters and existence of multiple parameter sets providing similar fit quality. Although global analysis over a vast array of data points allows to reduce parameter correlation, it is important in the fitting procedure to set bounds on the space of admissible parameter values. Specifically, $a_{1,2}$ and $n_{1,2}$ must satisfy the following condition $a_1 n_1 P + a_2 n_2 P \leq \Delta I_{max}$, where ΔI_{max} stands for limiting fluorescence increase observed at complete saturation of the binding centers. It should be noted at this point that special care was taken to ensure that the plateau in $\Delta I(Z)$ dependence (Fig. 3C) is not related to the inner filter effect arising from the increased adsorption of the incident and emitted light with elevating ThT concentration (Sulatskaya et al., 2011). Within the range of ThT concentrations used in our titration experiments fluorescence intensity proved to be linearly dependent on the dye optical density, that did not exceed 0.2. This implies that the plateau in the $\Delta I(Z)$ curve actually reflects saturation of ThT binding centers on apoA-I fibrils, rather than trivial re-absorption of the exciting or emitted light.

Likewise, taking into account that the ratio of ThT quantum yields in fibril-bound state and in a buffer cannot exceed 10^4 (since ThT quantum yield in water is ca. 10^{-4} (Sulatskaya et al., 2010)) the upper limit for $a_{1,2}$ (which is actually equal to instrumental factor)

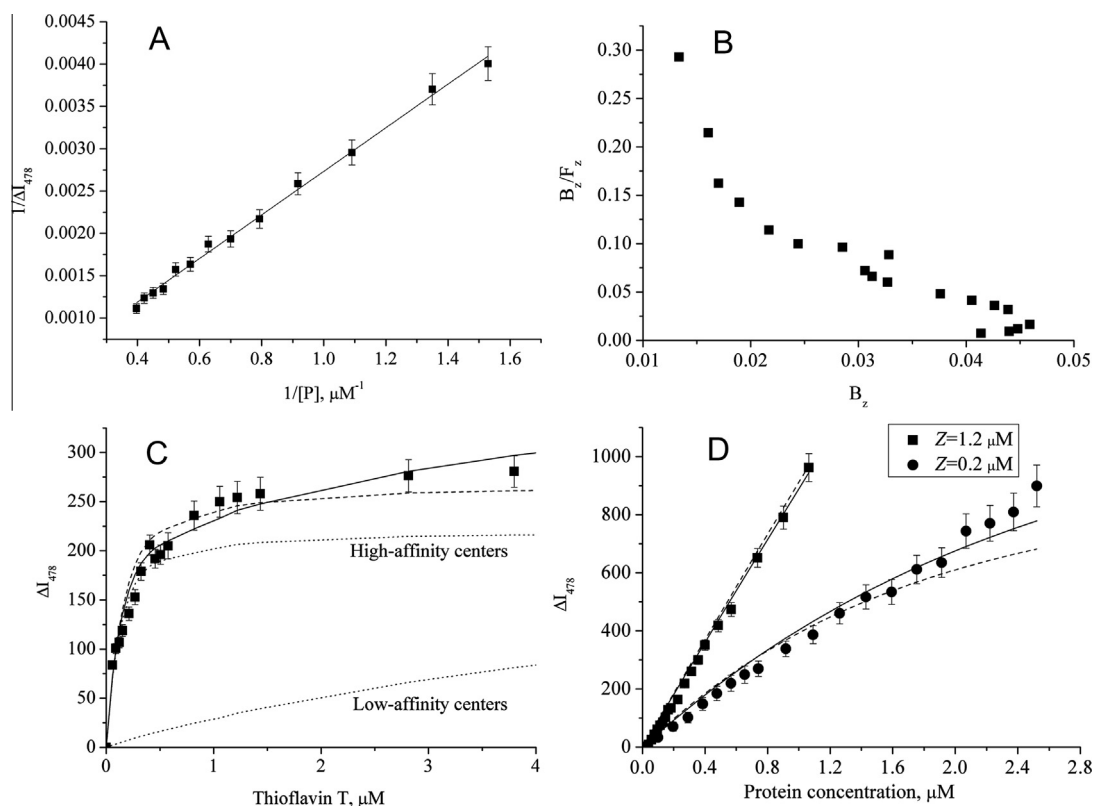


Fig. 3. Dye-fibril binding isotherms obtained by measuring the increase in ThT fluorescence intensity at 478 nm relative to that in buffer (ΔI_{478}): A – the double reciprocal plots for ThT titration by the protein. ThT concentration was 0.17 μM . B – Scatchard transform of $\Delta I_{478}(Z)$ binding curve. C – ΔI_{478} as a function of ThT concentration. Protein concentration was 0.35 μM . The contributions of ThT associated with high- and low-affinity sites are depicted by dot lines. Dash and solid lines represent theoretical curves calculated in terms of one- and two-sites binding models, respectively. D – ΔI_{478} as a function of protein concentration.

was estimated to be $\sim 1.1 \times 10^5$. Allowing for all these confinements, the non-linear regression analysis gave the following parameter set: $a_1 = (8.9 \pm 1.3) \times 10^3 \mu\text{M}^{-1}$, $K_{a1} = (6.2 \pm 0.7) \mu\text{M}^{-1}$, $n_1 = 0.1 \pm 0.02$ (high-affinity centers); $a_2 = (5.6 \pm 1.2) \times 10^3 \mu\text{M}^{-1}$, $K_{a2} = (0.14 \pm 0.03) \mu\text{M}^{-1}$, $n_2 = 0.17 \pm 0.03$, (low-affinity centers); $f = 1.39$. Using the above instrumental factor, the estimates of $a_{1,2}$ were converted into the values of quantum yield for fibril-bound ThT, that appeared to be ~ 0.08 for high-affinity centers and ~ 0.05 for low-affinity centers. The observed heterogeneity of ThT binding centers may arise from: (i) existence of structurally and compositionally different sites within fibrillar aggregates of a certain morphology and (ii) polymorphism intrinsic to most amyloid preparations. Indeed, as seen in Fig. 4A fibrils from 1-83/G26R apoA-I variant have smooth or twisted appearance indicative of their structural polymorphism.

3.2. Structural model of fibrillar apoA-I variant

The second step of the study was aimed at development of a putative structural model for fibrillar apoA-I variant consistent with the Trp–ThT distance constraints derived from the FRET measurements. To evaluate the aggregation tendency of 1–83 apoA-I N-terminal fragment, its sequence was scanned with AGGRESCAN (Conchillo-Sole et al., 2007), Zyggregator (Tartaglia and Vendruscolo, 2008) and TANGO (Linding et al., 2004) methods based on estimating the aggregation and beta-sheet propensities for individual amino acids. It appeared that the regions embracing the residues 14–21 and 53–58, 14–22 and 50–58, 14–23 and 53–57 (for AGGRESCAN, Zyggregator and TANGO algorithms, respectively) display the highest aggregation propensity. Moreover, the EPR spectroscopy analysis revealed that glycine replacement in apoA-I (G26R) leads to the extension of β -strand from 20–25 region in WT

protein, to a much longer β -strand comprising the residues 27–31, 41–52, and 53–56 which are characterized by specific β -structure patterns (Lagerstedt et al., 2007). Furthermore, recent X-ray crystallographic studies showed the apoA-I segment 44–55 to possess the high intrinsic propensity to β -sheet formation (Gursky et al., 2012). Consistent with this, a peptide comprising residues 46–59 of apoA-I was shown to aggregate to form amyloid-like fibrils (Wong et al., 2012). However, several lines of evidence, viz. (i) the presence of proline residues at positions 3, 4, 7, 66 and glycine at positions 35 and 39, (ii) the proteolytic accessibility of E34 and F57 (Lagerstedt et al., 2007) and (iii) TANGO prediction that the sequences 14–31 and 41–58 have the highest propensity to the formation of amphipathic β -sheets, allowed us to exclude the residues 1–13, 32–40 and 59–83 from the consideration of possible β -strand regions. As follows from the AFM results, the height of fibrils from N-terminal fragment of apoA-I is about 5–10 nm (Fig. 4A), while the total length of fully extended polypeptide is about twofold greater, ca. 28 nm. Taken together, all these rationales imply that protofilaments of apoA-I fibrils are likely to have β -strand–loop– β -strand structure, in which the polypeptides in the U-shape are registered in parallel, and the above tentative β -strands embracing 14–31 and 41–58 residues tend to form self-complementary steric zipper stabilized by van der Waals and hydrophobic interactions, as well as by the presumptive salt bridge between R27 and D48 of neighbouring strands. This assumption is in accord with the finding that Trp50 at C-terminal β -strand is buried within the fibril structure, as judged from the blue shift of Trp emission maximum of apoA-I variant and reduced Trp fluorescence quenching by iodide (Adachi et al., 2013). To verify the hypothesis about the involvement of R27–D48 salt bridge in stabilization of fibril structure, we compared ThT fluorescence kinetics for 1-83/G26R/W@8 and 1-83/G26R/D48A/W@8 apoA-I variants. Indeed, it appeared

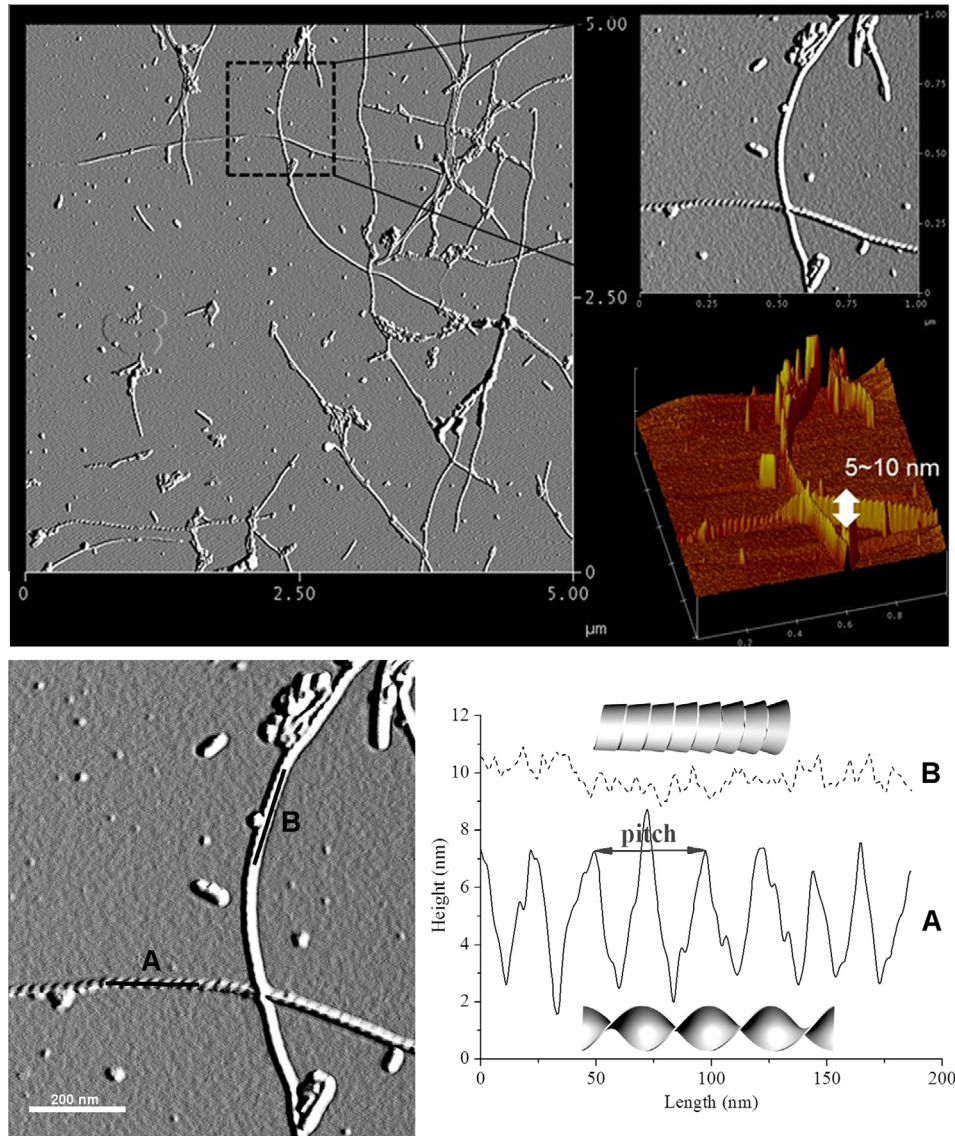


Fig. 4. AFM images of amyloid fibrils formed by 1-83/G26R apoA-I variant: A – images of $5 \mu\text{m} \times 5 \mu\text{m}$ and $1 \mu\text{m} \times 1 \mu\text{m}$ were obtained by amplitude mode, and image of the height was obtained by 3D height mode. B – Height profiles acquired over contour length for different polymorphs of apoA-I fibrils.

that substitution of negatively charged aspartic acid at position 48 for the neutral amino acid alanine prevents the increase in ThT fluorescence, indicating that fibril formation is substantially slowed down (Fig. 1). Moreover, CD measurements showed that incubation of 1-83/G26R(W@8), but not 1-83/G26R/D48A(W@8), is characterized by the transition to the minimum at 216 nm, indicative of a substantial population of β -sheet structure (Fig. 5). In addition, the assumption about salt bridge between residues R27 and D48 is corroborated by the effects of G26E, G26R and G26K mutations on apoA-I fibrillization (Adachi et al., 2013). Inhibition of fibril formation was observed for G26E, where salt bridge is presumably formed between the two adjacent oppositely charged residues (E26 and R27), excluding R27 from the interstrand salt bridge formation. Both mutations, D48A and G26E are likely to destabilize amyloid core, because, according to the proposed structural model, residue D48 (in the case of G26E mutation) and residue R27 (in the case of D48A mutation) would have energetically unfavorable orientation towards highly hydrophobic fibril interior. The G26R and G26K mutations, on the contrary, lead to the enhancement of amyloid fibril formation (Adachi et al., 2013). This effect could be the consequence of facilitation of R27–D48 salt bridge formation

because repulsion between similarly charged R26 (or K26) and R27 would favor orientation of R27 towards D48.

Based on the above considerations, a tentative starting structure for fibrillar apoA-I variant was created for four protein monomers using Rosetta and VMD software (Delano, 2005; Humphrey et al., 1996), as schematically depicted in Fig. 6.

3.3. Resonance energy transfer studies

All the above quantitative and qualitative information provided the basis for further FRET analysis of the examined system. Due to the overlap between Trp emission and ThT absorption spectra, the energy can be transferred between these fluorophores by a distance-dependent Förster mechanism. As illustrated in Fig. 7A, FRET manifests itself in the intensity decrease at the Trp emission maximum and a corresponding intensity increase at the ThT emission maximum. Relative quantum yield of the donor, calculated from the Eq. (1) after correction of the measured I_{DA} values for the sample dilution and inner filter effect, showed a nearly exponential decrease with ThT concentration, being virtually independent of the protein concentration (Fig. 7B). In an attempt to derive

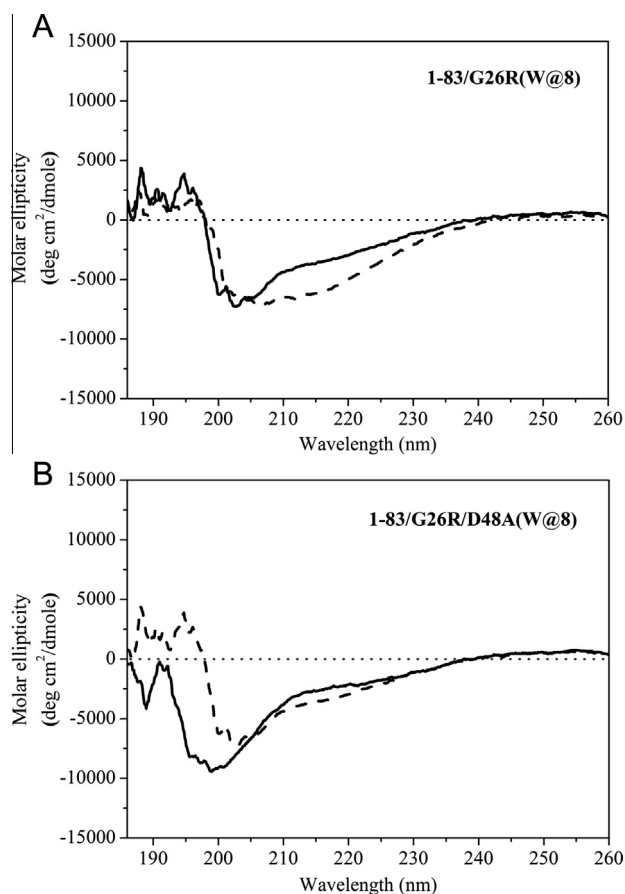


Fig. 5. Far-UV CD spectra of 1-83/G26R/W@8 (A) and 1-83/G26R/D48A/W@8 (B) variants before (solid line) and after incubation for 120 h (dashed line) at pH 7.4.

quantitative estimates for the donor-acceptor separation, the obtained FRET data were analyzed in terms of three theoretical approaches.

3.3.1. General approach

The first kind of FRET analysis makes use of the classical expression for distance dependence of FRET efficiency:

$$R = R_0(1/E - 1)^{1/6} \quad (9)$$

By introducing into this relationship the R_0 value indicated above for Trp–ThT pair (2.9 nm) and the highest measured E value, corresponding to saturation of the fibril binding centers by ThT, one obtains the average donor-acceptor distance $R \sim 4.3$ nm. This estimate

is valid only for the case when transition dipoles of donor and acceptor can adopt all orientations in a time short compared with the transfer time, since R_0 was calculated with the isotropic value of the orientation factor ($\kappa^2 = 0.67$). However, in highly anisotropic fibril structure fluorophores have limited freedom of motion and the isotropic condition is hardly satisfied. Such an uncertainty in the choice of orientation factor may lead to considerable ambiguities in the quantitative interpretation of FRET data. One way to circumvent this problem involves setting the upper and lower κ^2 limits using the information on the fluorophore rotational mobility derived from the anisotropy measurements. In terms of the formalism developed by (Dale et al. (1979)) the minimum (κ_{\min}^2) and maximum (κ_{\max}^2) κ^2 values are defined as:

$$\begin{aligned} \kappa_{\min}^2 &= 2/3(1 - 0.5(d_D + d_A)); & \kappa_{\max}^2 \\ &= 2/3(1 + d_D + d_A + 3d_Dd_A) \end{aligned} \quad (10)$$

here d_D and d_A are depolarization factors related to the steady-state (r) and fundamental (r_0) anisotropies of the donor and acceptor:

$$d_D = \left(\frac{r_D}{r_{0D}}\right)^{1/2}; \quad d_A = \left(\frac{r_A}{r_{0A}}\right)^{1/2} \quad (11)$$

Tryptophan absorbance in the range 250–300 nm is determined by the two electronic transitions 1L_a and 1L_b whose transition moments are orthogonally oriented (Valeur and Weber, 1977). The excitation wavelength of 296 nm used in our experiments predominantly populates the 1L_a state of the fluorophore (Albinsson et al., 1989) with the transition moment lying in the plane of the indole ring and fundamental anisotropy $r_{0D} = 0.3$ (Lakowicz, 2006). Steady-state anisotropy measurements yielded r_D and r_A values of 0.08 and 0.35, respectively, indicating that the Trp residue of the examined apoA-I variant rotates rather freely, while ThT mobility is substantially restricted upon dye-fibril binding. The lower and upper κ^2 limits calculated from Eqs. (10) and (11) with the above anisotropy values turned out to be $\kappa_{\min}^2 = 0.18$; $\kappa_{\max}^2 = 2.6$ (r_{0A} was taken as 0.4). Evaluation of the κ^2 bounds allowed us to obtain rough estimates for possible Trp–ThT distances: $R_{\min} = 3.5$ nm, $R_{\max} = 5.4$ nm.

3.3.2. FRET analysis ignoring fibril polymorphism

Next, it seemed reasonable to estimate Trp–ThT separation allowing for particular arrangement of these fluorophores within the fibril structure and assuming the existence of high- and low-affinity ThT binding sites in all types of fibrillar aggregates regardless of their morphology. According to the “channel” model of ThT–fibril binding, this dye tends to reside along surface side-chain grooves running parallel to the long fibril axis (Krebs et al., 2005; Biancalana et al., 2008; Teoh et al., 2011). As a first approximation, the application points of the donor emission and acceptor absorption transition moments were treated as lying along nearly parallel lines. Based on this assumption, the positions of donors and acceptors were

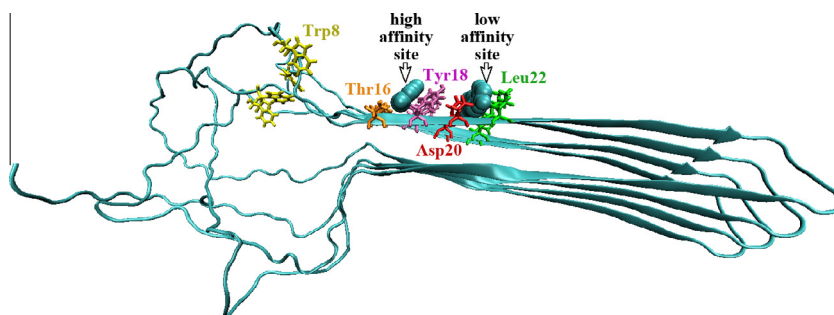


Fig. 6. 3D structure of tetrameric apoA-I variant 1-83/G26R/W@8 in a fibrillar state derived from Rosetta calculations. Shown in blue is ThT molecule, the amino acid residues are colored as: Thr 16 – orange, Tyr18 – mauve, Asp20 – red, Leu22 – green, Trp8 – yellow. (For interpretation of the references to colour in this figure legend, the reader is referred to the web version of this article.)

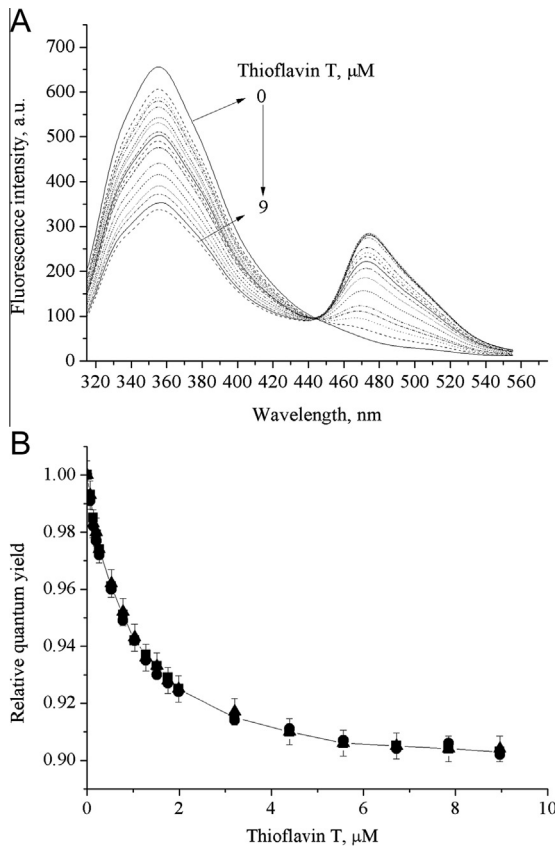


Fig. 7. FRET data for Trp–ThT donor–acceptor pair: A – emission spectra of fibrillar single Trp apoA-I variant recorded at increasing ThT concentrations. Protein concentration was 3 μM . B – Relative quantum yield of apoA-I Trp as a function of ThT concentration. Protein concentration was 1 μM (●), 2 μM (▲) or 3 μM (■).

generated in a virtual elongated cell, taking the separation between the adjacent Trp residues equal to the interstrand distance in the β -sheet (0.47 nm). The relative quantum yield averaged over all donors was calculated from the fluorophore coordinates as:

$$Q_r = \frac{1}{N_D} \sum_{j=1}^{N_D} \left[1 + \sum_{i=1}^{N_{AC}} \left(\frac{R_0}{r_{ij}} \right)^6 \right]^{-1} \quad (12)$$

where N_D , N_{AC} stand for the number of donors and acceptors, respectively. The N_{AC} value was determined using the above ThT binding parameters. Under the employed conditions of FRET measurements the amount of bound ThT per protein monomer (B_z/P) was found to be 0.098 (one ThT molecule per ~ 10 protein monomers) and 0.092 (one ThT molecule per ~ 11 protein monomers) for the high- and low-affinity binding sites, respectively. This simulation-based approach yielded possible combinations of distances between Trp and ThT linear arrays ($R_{1,2}$) concordant with the experimentally measured energy transfer efficiency. Presented in Table 1 are the distance estimates obtained with a common assumption of random reorientation of donors and acceptors ($\kappa^2 = 0.67$), and the bounds for these parameters calculated using the above depolarization-based approach (Eqs. (10) and (11)).

Since highly specific ThT–fibril binding is thought to involve dye incorporation into superficially located grooves, solvent-exposed residues on each β -strand can in principle be implicated in the dye accommodation. As follows from the above structural model, the grooves that could serve as potential binding sites for ThT, are formed by residues L14_T16_Y18_D20_L22_D24_R26_D28_V30 in the N-terminal β -sheet layer and by residues Q41_N43_K45_L47_N49_D51, S52_T54_T56_S58 in the C-terminal β -sheet layer.

Table 1

Possible separations between Trp and ThT located at high-affinity (R_1 , nm) and low-affinity (R_2 , nm) centers of fibrillar apoA-I variant 1-83/G26R/W@8.

Parameter set	$R_{1\min}$	$R_{1\max}$	$R_{2\min}$	$R_{2\max}$	$\Delta R_{21} (\kappa^2_{\min})^*$	$\Delta R_{21} (\kappa^2_{\max})^*$
S1	3.5	5.4	5.6	8.9	2.1	3.5
S2	3.6	5.6	4.8	7.5	1.2	1.9
S3	3.9	6.1	4.0	6.3	0.1	0.2
S4	4.1	6.4	3.9	6.0	−0.2	−0.4
S5	6.3	9.8	3.5	5.5	−2.8	−4.3

* $\Delta R_{21} = R_2 - R_1$.

However, these sites seem to be non-equivalent in terms of their ThT association specificity. Increasing evidence indicates that ThT has binding preference for grooves lined with aromatic residues, particularly, Tyr and Phe (Wu et al., 2008, 2009; Biancalana et al., 2009). The factors, such as ability to π -stacking interactions and large hydrophobic surfaces provided by aromatic amino acids are supposed to play a crucial role in immobilizing the two aromatic rings of ThT and the subsequent fluorescence enhancement (Stsiapura et al., 2007; Biancalana and Koide, 2010). Furthermore, it has been demonstrated that ThT displays high affinity for hydrophobic amino acid residues (Wu et al., 2011). In view of this, C-terminal β -sheet layer which is devoid of aromatic amino acid residues and contains only one hydrophobic residue (L47), seems to be much less favorable for ThT accommodation than N-terminal β -sheet layer. All these rationales, together with the assumption that negative charge of Asp may be of value in targeting positively charged ThT molecule to the surface of apoA-I fibrils, allowed us to define possible ThT binding sites, viz. the grooves T16_Y18 (G1) and Y18_D20 (G2) for high-affinity centers and the grooves D20_L22 (G3), L22_D24 (G4) and D28_V30 (G5) for low-affinity centers. Taking the propagation of an extended polypeptide chain as ~ 0.35 nm per residue and Trp radius as ~ 0.32 nm one obtains that maximum separation between Trp8 and the above grooves (R_{W8G}) lies between 3.5 and 7.6 nm (Table 2). Although Trp8 is located outside of the β -sheet core in potentially flexible loop region, the grooves can be considered as separated by a fixed distance because of rigidity of fibril structure. The following analysis was intended to ascertain what spatial separations of G1–G5 agree with the parameter sets derived from the simulation-based FRET data fitting. Comparison of the estimates presented in Tables 1 and 2 show that location of high-affinity sites on G1 is consistent with $R_{1\min}$ from the parameter sets S1 and S2, while R_{W8G} is closer to $R_{1\min}$ from the sets S3 and S4. On the other hand, comparing the range of possible ΔR_{21} values (Table 1) with the intergroove separations (Table 2), one can see that the distances from G1 to G3 and G4 are consistent with ΔR_{21} bounds obtained for the sets S1 and S2. However, this is not the case for G2, because no of the grooves G3–G5 is separated from G2 by the distance compatible with ΔR_{21} estimates acquired for the sets S3 and S4. All these considerations point to the groove T16_Y18 as the most likely candidate for high-affinity ThT binding centers, while the grooves D20_L22 and L22_D24 can serve as low-affinity ThT binding sites.

3.3.3. FRET analysis allowing for fibril polymorphism

Finally, we made an attempt to extend FRET analysis to the case where high- and low-affinity ThT binding sites are located on distinct fibril polymorphs. Analysis of the height profiles over contour length performed for two types of apoA-I fibrils (Fig. 4B) strongly suggests that different polymorphs are represented by twisted ribbons (fibril in a nearly horizontal orientation) and helical ribbons (fibril in a nearly vertical orientation, Fig. 4A, right image). Spatial distribution of Trp and ThT moieties in the twisted ribbon structure can be described by the following general expressions

Table 2
Inter-groove separations in fibrillar apoA-I variant 1-83/G26R/W@8.

Groove	Maximum distance from Trp8, nm	Distance from G1, nm	Distance from G2, nm	Curvature, κ_{TR}
G1, T16_Y18	3.5	0	0.7	0.023
G2, Y18_D20	4.2	0.7	0	0.013
G3, D20_L22	4.9	1.4	0.7	0.002
G4, L22_D24	5.6	2.1	1.4	-0.009
G5, D28_V30	7.6	4.1	3.4	-0.037

that define the coordinates of donors ($X_{D_i}, Y_{D_i}, Z_{D_i}$) and acceptors ($X_{A_j}, Y_{A_j}, Z_{A_j}$):

$$\begin{aligned} X_{D_i} &= 0.5w \cos\left(\frac{2\pi d_m i}{P_{TR}}\right); & Y_{D_i} &= 0.5w \sin\left(\frac{2\pi d_m i}{P_{TR}}\right); & Z_{D_i} &= d_m i; \\ X_{A_j} &= (0.5w - d_{TR}) \cos\left(\frac{2\pi d_m j}{P_{TR}}\right); & Y_{A_j} &= (0.5w - d_{TR}) \sin\left(\frac{2\pi d_m j}{P_{TR}}\right); & Z_{A_j} &= n_{TR} d_m j; \end{aligned} \quad (13)$$

where w , width of fibril core; P_{TR} , pitch; d_m , vertical distance between protein monomers (along z-axis); n_{TR} , the number of protein monomers per one acceptor molecule; d_{TR} , Trp–ThT distance in twisted ribbon structure. Similar relationships can be employed to generate the coordinates of donors ($X_{D_k}, Y_{D_k}, Z_{D_k}$) and acceptors ($X_{A_l}, Y_{A_l}, Z_{A_l}$) in helical ribbon structure:

$$\begin{aligned} X_{D_k} &= r_h \cos\left(\frac{2\pi d_h k}{P_{HR}}\right); & Y_{D_k} &= 0.5w \sin\left(\frac{2\pi d_h k}{P_{HR}}\right); \\ Z_{D_k} &= d_h k; & P_{HR} &= 2\pi r_h \tan \psi; & X_{A_l} &= r_h \cos\left(\frac{2\pi d_h l}{P_{HR}}\right); \\ Y_{A_l} &= r_h \sin\left(\frac{2\pi d_h l}{P_{HR}}\right); & Z_{A_l} &= \frac{d_{HR}}{\cos \psi} + n_{HR} d_h l; \end{aligned} \quad (14)$$

here r_h , helix radius; P_{HR} , pitch; ψ , pitch angle; $d_h = d_m \sin \psi$, distance between protein monomers along z-axis, coinciding with helix axis; n_{HR} , the number of protein monomers per one acceptor molecule; d_{HR} , Trp–ThT distance in helical ribbon structure. Eqs. (13) and (14), being combined with Eq. (12) allowed us to simulate FRET in two types of fibril polymorphs with the following sets of structural parameters derived from AFM data for twisted ribbon ($w = 10$ nm; $P_{TR} = 50$ nm) and helical ribbon ($r_h = 5$ nm; $\psi = 70^\circ$). The value of d_m was taken as 0.47 nm, the interstrand distance in β -sheet, whereas n_{TR} and n_{HR} were obtained from the above binding data, $n_{TR} = 11$ and $n_{HR} = 10$. Notably, we supposed that high-affinity ThT binding centers reside on helical ribbon polymorphs, while low-affinity centers are located on twisted ribbon polymorphs. To substantiate this assumption, we resorted to the quantity, such as surface curvature, that for helical (κ_{HR}) and twisted (κ_{TR}) ribbons is given by:

$$\kappa_{HR} = \frac{r_h}{r_h^2 + (P_{HR}/2\pi)^2}; \quad \kappa_{TR} = \frac{0.5w - d_{TR}}{(0.5w - d_{TR})^2 + (P_{TR}/2\pi)^2} \quad (15)$$

As follows from Eq. (15), helical ribbon fibrils has constant curvature, ~ 0.02 , while curvature of twisted ribbon fibrils varies from 0.06 to 0. For this reason, the probability to adopt a nearly planar motionally restricted conformation seems to be higher for ThT molecules associating with the grooves on helical ribbon structure. Based on these considerations, we found the sets (d_{HR}, d_{TR}) providing the best agreement between theoretical and experimental Q_f values. Presented in Table 3 are d_{HR} and d_{TR} estimates obtained with $\kappa^2 = 0.67$, and the limits for these parameters calculated from Eqs. (10) and (11). It appeared that the widest possible limits recovered for d_{HR} , 0.6–3.8 nm, are consistent only with ThT location in the groove G1 (T16_Y18), while d_{TR} limits (3.1–7.8 nm) cover all aforementioned grooves G1–G5 (Table 2). Thus, both kinds of FRET anal-

Table 3
Possible separations between Trp and ThT located at helical ribbon fibrils (d_{HR}) and twisted ribbon fibrils (d_{TR}) of apoA-I variant 1-83/G26R/W@8.

d_{HR} , nm	d_{HRmin}	d_{HRmax}	d_{TR} , nm	d_{TRmin}^*	d_{TRmax}^*
3.0	2.4	3.8	3.8	3.1	4.8
2.5	2.0	3.1	4.0	3.2	5.0
0.8	0.6	1.0	5.0	4.0	6.2
2.6	2.1	3.3	6.0	4.8	7.5
2.9	2.3	3.6	6.2	5.0	7.8

ysis, neglecting and taking into account the existence of distinct polymorphic states of fibrillar apoA-I variant provide support for the assumption that the groove lined with T16 and Y18 is involved in high-affinity ThT–fibril binding. As regards to low-affinity centers, the groove G3 (D20_L22) having the lowest curvature (~ 0.002) within twisted ribbon fibrils (Table 2) seems to be most suitable for ThT accommodation in a nearly planar conformation (Fig. 6).

To summarize, the present study was undertaken to elucidate the nature of interactions between an amyloidogenic variant of N-terminal fragment of apoA-I (1-83/G26R/W@8) and the most prominent amyloid marker ThT. For the first time, to our knowledge, FRET analysis was employed to evaluate Trp–ThT separation within the structure of apoA-I fibrils. Quantitative interpretation of the results of double fluorimetric titration revealed two distinct classes of ThT binding sites with similar stoichiometries (one ThT molecule per 10–11 protein monomers), but different binding affinities corresponding to the Gibbs free energy changes of ~ -38 and -29 kJ/mol. The distance constraints recovered from Trp8–ThT FRET analysis turned out to be consistent with the proposed β -strand–loop– β -strand structural model of 1-83/G26R/W@8 apoA-I fibrils. The N-terminal β -sheet layer enriched with aromatic and hydrophobic amino acid residues was assumed to provide the grooves favorable for ThT accommodation. Extended FRET analysis allowing for heterogeneity of ThT binding centers and fibril polymorphism suggests that high-affinity ThT binding sites reside at the groove created by T16 and Y18, while low-affinity sites are lined up at the grooves D20_L22.

The proposed structural model of fibrillar N-terminal fragment 1-83/G26R/W@8 may prove of importance as a starting point for further in-depth characterization of fibrillar forms of apoA-I.

Acknowledgments

This work was supported by the grant from the Fundamental Research State Fund of Ukraine (project number F54.4/015) and Grant-in-Aid for Scientific Research (25293006 and 25670014) from Japan Society for the Promotion of Science.

References

- Adachi, E., Nakajima, H., Mizuguchi, C., Dhanasekaran, P., Kawashima, H., Nagao, K., Akaji, K., Lund-Katz, S., Phillips, M.C., Saito, H., 2013. Dual role of an N-terminal amyloidogenic mutation in apolipoprotein A-I: destabilization of helix bundle and enhancement of fibril formation. *J. Biol. Chem.* 288, 2848–2856.
- Albinsson, B., Kubista, M., Norden, B., Thulstrup, E., 1989. Near-ultraviolet electronic transitions of the tryptophan fluorophore: linear dichroism, fluorescence

- anisotropy, and magnetic circular dichroism spectra of some indole derivatives. *J. Phys. Chem.* 93, 6646–6654.
- Biancalana, M., Makabe, K., Koide, A., Koide, S., 2008. Aromatic cross-strand ladders control the structure and stability of beta-rich peptide self-assembly mimics. *J. Mol. Biol.* 383, 205–213.
- Biancalana, M., Makabe, K., Koide, A., Koide, S., 2009. Molecular mechanism of Thioflavin T binding to the surface of beta-rich peptide self-assemblies. *J. Mol. Biol.* 385, 1052–1063.
- Biancalana, M., Koide, S., 2010. Molecular mechanism of Thioflavin T binding to amyloid fibrils. *Biochim. Biophys. Acta* 1804, 1405–1412.
- Bulychev, A.A., Verchoturov, V.N., Gulaev, B.A., 1988. *Current Methods of Biophysical Studies*. Vyschaya Shkola, Moscow.
- Conchillo-Sole, O., de Groot, N.S., Avilés, F., Vendrell, J., Daura, X., Ventura, S., 2007. AGGRESCAN: a server for the prediction and evaluation of “hot spots” of aggregation in polypeptides. *BMC Bioinformatics* 8, 65.
- Dale, R., Eisinger, J., Blumberg, W., 1979. The orientational freedom of molecular probes. The orientation factor in intramolecular energy transfer. *Biophys. J.* 26, 161–194.
- Delano, W.L., 2005. The case for open-source software in drug discovery. *Drug Discov. Today* 10, 213–217.
- Groenning, M., 2010. Binding mode of Thioflavin T and other molecular probes in the context of amyloid fibrils—current status. *J. Chem. Biol.* 3, 1–18.
- Gursky, O., Mei, X., Atkinson, D., 2012. The crystal structure of the C-terminal truncated apolipoprotein A-I sheds new light on amyloid formation by the N-terminal fragment. *Biochemistry* 51, 10–18.
- Hawe, A., Sutter, M., Jiskoot, W., 2008. Extrinsic fluorescent dyes as tools for protein characterization. *Pharm. Res.* 25, 1487–1499.
- Humphrey, W., Dalke, A., Schulten, K., 1996. VMD: visual molecular dynamics. *J. Mol. Graph.* 14, 33–38.
- Idicula-Thomas, S., Balaji, P.V., 2007. Protein aggregation: a perspective from amyloid and inclusion body formation. *Curr. Sci.* 92, 758–767.
- Joy, T., Wang, J., Hahn, A., Hegele, R.A., 2003. ApoA-I related amyloidosis: a case report and literature review. *Clin. Biochem.* 36, 641–645.
- Knowles, T.P., Buehler, M., 2011. Nanomechanics of functional and pathological amyloid materials. *Nat. Nanotechnol.* 6, 469–479.
- Koradi, R., Billeter, M., Wuthrich, K., 1996. MOLMOL: a program for display and analysis of macromolecular structures. *J. Mol. Graph.* 14, 51–55.
- Krebs, M.R., Bromley, E.H., Donald, A.M., 2005. The binding of Thioflavin T to amyloid fibrils: localization and implications. *J. Struct. Biol.* 149, 30–37.
- Lagerstedt, J.O., Cavigliolo, G., Roberts, L.M., Hong, H.S., Jin, L.W., Fitzgerald, P.G., Oda, M.N., Voss, J.C., 2007. Mapping the structural transition in an amyloidogenic apolipoprotein A-I. *Biochemistry* 46, 9693–9699.
- Lakowicz, J.R., 2006. *Principles of Fluorescent Spectroscopy*, 3rd ed. Springer, New York.
- LeVine III, H., 1993. Thioflavin T interaction with synthetic Alzheimer's disease A β – amyloid peptides: detection of amyloid aggregation in solution. *Protein Sci.* 2, 404–410.
- Linding, R., Schymkowitz, J., Rousseau, F., Diella, F., Serrano, L., 2004. A comparative study of the relationship between protein structure and beta-aggregation in globular and intrinsically disordered proteins. *J. Mol. Biol.* 342, 345–353.
- Mankar, S., Anoop, A., Sen, S., Maji, S.K., 2011. Nanomaterials: amyloids reflect their brighter side. *Nano Rev.* 2, 6032.
- Makin, O.S., Serpell, L.C., 2005. Structures for amyloid fibrils. *FEBS J.* 272, 5950–5961.
- Naiki, H., Higuchi, K., Hosokawa, M., Takeda, T., 1989. Fluorometric determination of amyloid fibrils in vitro using the fluorescent dye, Thioflavin T. *Anal. Biochem.* 177, 244–249.
- Nelson, R., Eisenberg, D., 2006. Recent atomic models of amyloid fibril structure. *Curr. Opin. Struct. Biol.* 16, 260–265.
- Nichols, W.C., Gregg, R.E., Brewer, H.B., Benson, M.D., 1990. A mutation in apolipoprotein A-I in the Iowa type of familial amyloidotic polyneuropathy. *Genomics* 8, 318–323.
- Phillips, M.C., 2013. New insights into the determination of HDL structure by apolipoproteins: Thematic Review Series: High Density Lipoprotein Structure, Function, and Metabolism. *J. Lipid. Res.* 54, 2034–2048.
- Selvin, P.R., 1996. Lanthanide-based resonance energy transfer. *IEEE J. Sel. Top. Quantum Electron.* 2, 1077–1087.
- Stefani, M., 2004. Protein misfolding and aggregation: new examples in medicine and biology of the dark side of the protein world. *Biochim. Biophys. Acta* 1739, 5–25.
- Stsiapura, V.I., Maskevich, A.A., Kuznetsova, I.M., 2007. Computational study of Thioflavin T torsional relaxation in the excited state. *J. Phys. Chem. A* 111, 4829–4835.
- Sulatskaya, A.I., Maskevich, A.A., Kuznetsova, I.M., Uversky, V.N., Turoverov, K.K., 2010. Fluorescence quantum yield of Thioflavin T in rigid isotropic solution and incorporated into the amyloid fibrils. *PLoS One* 5, e15385.
- Sulatskaya, A.I., Kuznetsova, I.M., Turoverov, K.K., 2011. Interaction of Thioflavin T with amyloid fibrils: stoichiometry and affinity of dye binding, absorption spectra of bound dye. *J. Phys. Chem. B* 115, 11519–11524.
- Tartaglia, G.G., Vendruscolo, M., 2008. The Zyggregator method for predicting protein aggregation propensities. *Chem. Soc. Rev.* 37, 1395–1401.
- Teoh, C.L., Pham, C.L., Todorova, N., Hung, A., Lincoln, C.N., Lees, E., Lam, Y.H., Binger, K.J., Thomson, N.H., Radford, S.E., Smith, T.A., Müller, S.A., Engel, A., Griffin, M.D., Yarovsky, I., Gooley, P.R., Howlett, G.J., 2011. A structural model for apolipoprotein C-II amyloid fibrils: experimental characterization and molecular dynamics simulations. *J. Mol. Biol.* 4, 1246–1266.
- Valeur, B., Weber, G., 1977. Resolution of the fluorescence excitation spectrum of indole into 1L_a and 1L_b excitation bands. *Photochem. Photobiol.* 25, 441–444.
- Wong, Y.Q., Binger, K.J., Howlett, G.J., Griffin, M.D., 2012. Identification of an amyloid fibril forming peptide comprising residues 46–59 of apolipoprotein A-I. *FEBS Lett.* 586, 1754–1758.
- Wu, C., Wang, Z., Lei, H., Duan, Y., Bowers, M.T., Shea, J.E., 2008. The binding of Thioflavin T and its neutral analog BTA-1 to protofibrils of the Alzheimer's disease A β (16–22) peptide probed by molecular dynamics simulations. *J. Mol. Biol.* 384, 718–729.
- Wu, C., Biancalana, M., Koide, S., Shea, J.E., 2009. Binding modes of Thioflavin T to the single-layer beta-sheet of the peptide self-assembly mimics. *J. Mol. Biol.* 394, 627–633.
- Wu, C., Bowers, M.T., Shea, J.E., 2011. On the origin of the stronger binding of PIB over Thioflavin T to protofibrils of the Alzheimer amyloid- β peptide: a molecular dynamics study. *Biophys. J.* 100, 1316–1324.
- Zerovnik, E., 2002. Amyloid-fibril formation. Proposed mechanisms and relevance to conformational disease. *Eur. J. Biochem.* 269, 3362–3371.